Phononic Quantum Networks of Solid-State Spins with Alternating and Frequency-Selective Waveguides

Mark C. Kuzyk and Hailin Wang

Department of Physics, University of Oregon, Eugene, OR 97403, USA

Abstract

We develop a quantum network architecture, for which any two neighboring nodes and the communication channel between them can form a closed subsystem. This architecture is implemented in a phononic network of solid-state spins in diamond, in which nanomechanical resonators couple to color centers through phonon-assisted transitions. A key element of the implementation is the use of alternating phononic crystal waveguides that feature specially-designed band gaps, enabling alternating, frequency-selective coupling between mechanical resonators. The implementation also includes quantum state transfer between single spins or spin ensembles in neighboring resonators. An ensemble-spin based protocol, which requires a special ratio between the spin-mechanical and waveguide-resonator coupling rates, can be independent of the initial states of all the mechanical modes involved and thus be robust against the thermal environment. The proposed phononic network overcomes the inherent obstacles in scaling phononic quantum networks and avoids the technical difficulty of employing chiral spin-phonon interactions, providing a promising route for developing quantum computers using robust solid-state spin qubits.

I. INTRODUCTION

Photons are excellent carriers of quantum information and are the ideal choice for long distance quantum communications and networks[1-5]. For on-chip communications and networks, there are, however, a few inherent limitations. For example, the speed of light can be too fast for communications over short distances, such as a few hundred micrometers or less. Scattering losses of electromagnetic waves into vacuum can be excessive even with state-of-the-art nanofabrication technologies, which severely limits the photon lifetime in nano-optical systems such as photonic crystal optical resonators.

In comparison, phonons, which are the quanta of mechanical waves, feature several distinct advantages for on-chip communications[6-8]. The speed of sound is about five orders of magnitude slower than the speed of light. Mechanical waves cannot propagate in vacuum and thus are not subject to scattering or radiation losses into vacuum. The relatively long acoustic wavelength also makes it easier to fabricate phononic nanostructures for confining and guiding acoustic waves on a chip.

The primary function of a quantum network is to enable high-fidelity quantum state transfer between two neighboring quantum nodes. This can take place in a cascaded network[9], for which the coupling between neighboring quantum nodes is *unidirectional*[10]. Quantum state transfer protocols that are robust against thermal noise in the communication channel have been proposed recently for cascaded networks[11,12]. Cascaded optical quantum networks can be realized with chiral optical interactions[13,14], as demonstrated with atoms and quantum dots[15,16]. The lack of easily accessible chiral acoustic processes, however, makes it difficult to implement cascaded phononic quantum networks[6,17].

Furthermore, there are two inherent obstacles in scaling up a phononic network. First of all, the spin-mechanical coupling rate at the single-phonon level scales with the zero-point fluctuation of the mechanical system, which is proportional to $1/\sqrt{m}$ with m being the mass of the mechanical system. The larger the network is, the smaller the single-phonon coupling rate usually becomes. Secondly, nearest neighbor coupling of a large number of mechanical resonators can lead to the formation of spectrally-dense mechanical modes, causing crosstalk between the collective mechanical modes. These problems are well known in ion trap quantum computers[18], for which phonon-mediated interactions play an essential role. A solution to these problems is to

build phononic networks using *closed mechanical subsystems*. An apparent difficulty is to enable quantum state transfer between the seemingly closed subsystems.

In this paper, we propose a general and conceptually-simple architecture for quantum networks that feature *closed subsystems*. This architecture employs at least two frequencies for communications and exploits *alternating*, *frequency-selective* waveguides. As illustrated schematically in Fig. 1a, each quantum node couples to two waveguides, A and B, which allow signal propagation at frequencies near ω_A and ω_B , but forbid signal propagation at frequencies near ω_B and ω_A , respectively. This special frequency selectivity of the alternating waveguides can make any two neighboring nodes and the waveguide between them a closed subsystem, as highlighted in Fig. 1a. For a phononic quantum network of solid state spins, this architecture can be implemented with quantum nodes, in which a spin system couples selectively to two mechanical resonator modes with frequency ω_A and ω_B . This phononic quantum network can also be viewed as closed mechanical subsystems coupled together via the spins, as shown schematically in Fig. 1b. In this network, high-fidelity quantum state transfer between the neighboring spin systems can take place via the closed mechanical subsystems.

We describe an implementation of this architecture employing diamond color centers, nanomechanical resonators, and phononic crystal waveguides. In this implementation, color centers featuring robust spin qubits couple to vibrations of nanomechanical resonators through sideband (i.e. phonon-assisted) transitions driven by external optical or microwave fields[19]. Communications between these spin-mechanical resonators take place via alternating phononic crystal waveguides[20]. A key feature of the network is specially-designed band gaps in the phononic crystal waveguides, which enable frequency-selective coupling. In addition, the entire network can be embedded in a phononic crystal lattice, which isolates and protects the network from the surrounding mechanical environment. Note that diamond phononic crystals and optomechanical crystals, which are technically more demanding than diamond phononic crystals in terms of nanofabrication, have already been successfully realized[21-23].

We also outline two schemes for quantum state transfer between spin systems in neighboring resonators. One scheme relies on strong spin-mechanical coupling of a single spin. The other employs spin ensembles for the quantum state transfer and approximates the spin ensemble as a bosonic oscillator[11,12]. Both schemes can be robust against thermal phonons in the phononic waveguide.

Solid state spin systems such as negatively-charged nitrogen vacancy (NV) centers in diamond have emerged as a promising qubit system for quantum information processing[24-26]. High fidelity quantum control of individual spin qubits via microwave or optical transitions has been well established[27-33]. Photonic networks of NV centers have also been proposed[34-36]. The phononic quantum network described in this paper can potentially enable a scalable, chipbased experimental platform for developing quantum computers using robust solid-state spin qubits.

II. PHONONIC QUANTUM NETWORKS

The proposed phononic network consists of diamond-based spin-mechanical resonators that couple spin qubits in diamond to relevant mechanical modes, phononic crystal waveguides with suitable energy gaps and waveguide modes, and a two-dimensional (2D) phononic crystal lattice that protects the mechanical modes involved in the phononic network. For numerical calculations, we assume that the phononic network is fabricated from a diamond membrane with a thickness of 300 nm. In addition to NV centers, other color centers in diamond, such as silicon vacancy (SiV) or germanium vacancy (GeV) centers[37-40], can also be used in the phononic network. High quality NV, SiV, and GeV centers can be created in diamond through ion implantation, followed by elaborate thermal annealing and surface treatment[41,42].

A. Spin-Mechanical resonators

The elementary unit or node in our quantum network is a spin-mechanical resonator, in which spin qubits couple to mechanical resonator modes in a thin, rectangular diamond plate. Calculations of mechanical normal modes in the diamond plate are discussed in detail in the appendix. We are interested in mechanical compression modes that are symmetric with respect to the median plane of the plate (the so-called symmetric modes). Figure 2a shows, as an example, the displacement pattern of a fifth order compression mode.

Coherent interactions between electron spin states of a NV center and long-wavelength mechanical vibrations of the diamond lattice have been experimentally explored via either ground-state or excited-state strain coupling[19,43-53]. The orbital degrees of freedom of a NV center can couple strongly to the long-wavelength mechanical vibrations via the excited states. As a result, the excited-state strain coupling for a NV center is about five orders of magnitude stronger

than the ground-state strain coupling[53-55]. For defect centers such as SiV and GeV centers, strong coupling between the orbital degrees of freedom and the mechanical vibrations can also take place through the ground states[56].

As illustrated in Fig. 2b, we control the coupling between the ground spin states of the NV center and the relevant mechanical mode through a resonant Raman process that consists of a sideband (or phonon-assisted) optical transition as well as a direct dipole optical transition. The Raman process is driven and controlled by two external optical fields. The interaction Hamiltonian is given by [52]

$$V = \hbar \frac{\Omega_{-}}{2} \frac{g_{s}}{\omega_{m}} (\hat{a}e^{i(\Delta_{-}-\omega_{m})t} \mid e > < -|+h.c.) + \hbar \frac{\Omega_{+}}{2} (e^{i\Delta_{+}t} \mid e > < +|+h.c.),$$
(1)

where $g_s = Dk_m x_{zpf}$, D is the deformation potential, x_{zpf} is the zero-point fluctuation, k_m is the phonon wavevector, Ω_+ and Ω_- are the optical Rabi frequencies and Δ_+ and Δ_- are the effective dipole detunings for the two respective optical transitions, and \hat{a} is the annihilation operator for a mechanical mode with frequency ω_m . For a NV center, the $m_s = \pm 1$ ground spin states can serve as states $|\pm\rangle$ and the A_2 state can serve as state $|e\rangle$ [57].

The use of the sideband transitions, instead of resonant transitions, enables the selective coupling of an electron spin to any relevant mechanical mode, which is an essential requirement for the implementation of the proposed network architecture. Specifically, we can couple the electron spin states to a mechanical mode with frequency ω_m by setting the detuning between the two optical driving fields according to the Raman resonant condition, $\Delta_- - \omega_m = \Delta_+$. To avoid the population of the excited state, we can also exploit a combination of techniques, such as dark states, shortcuts to adiabatic passage[58,59], Magnus expansions[60], as well as large dipole detuning. Excited-state mediated spin-mechanical coupling via a dark state has already been demonstrated in an earlier experimental study[52].

Note that for negatively charged SiV or GeV centers that feature strong ground-state strain coupling, the spin-mechanical coupling can also be driven by microwave sideband transitions between the ground spin states. In addition, the coupling schemes discussed in [17] can also be adopted.

B. Phononic crystal waveguides and alternating, frequency-selective coupling

We use phononic crystal waveguides, which are one-dimensional (1D) phononic crystals consisting of a periodic array of holes in a beam (see Fig. 3a), to network together a series of spin-mechanical resonators. In a simple picture, mechanical vibrations in a resonator excite propagating mechanical waves in the adjacent phononic waveguides[20]. Conversely, mechanical waves in the phononic waveguide also excite vibrations in the adjacent mechanical resonators.

A suitable design of the phononic crystal waveguides can enable alternating, frequency-selective coupling for the phononic network. As shown in Fig. 3a, a spin-mechanical resonator couples to two phononic waveguides, A and B, that feature an array of elliptical holes with different periods. The phononic band structure of each waveguide shows a sizable band gap for the symmetric mechanical modes (see Fig. 3b). The center of the band gap for waveguide B, which features a shorter period, is higher in frequency than that for waveguide A, which features a longer period. For this design, the two band gaps have two non-overlapping spectral regions, as highlighted by the grey shaded areas in Fig. 3b. We use waveguide modes and resonator modes in these non-overlapping regions for quantum state transfer between spin systems in neighboring quantum nodes.

Specifically, for the resonator-waveguide design shown in Fig. 3a, a higher frequency resonator mode with $\omega_A/2\pi=1.6332$ GHz, which is a fifth order compression mode of the resonator and is in the band gap of waveguide B (see Fig. 3b), couples resonantly to a mode in waveguide A. A lower frequency resonator mode with $\omega_B/2\pi=0.9133$ GHz, which is a third order compression mode and is in the band gap of waveguide A (see Fig. 3b), couples resonantly to a mode in waveguide B. This design effectively realizes the network architecture shown in Fig. 1b.

Because of the alternating, frequency-selective coupling, any two neighboring resonators and the waveguide between them can form a closed subsystem. The relevant waveguide modes are thus discrete standing wave modes. For a relatively short waveguide, the frequency spacing of these modes can be large compared with other relevant frequency scales and the waveguide can thus behave like a single-mode mechanical oscillator. In this limit, we can treat the closed mechanical subsystem shown in Fig. 1b as a three-mode system. The appendix discusses in detail numerical calculations of the normal modes of the three-mode subsystem and, in particular, the coupling rate, g, between the resonator and the waveguide modes. Depending on the specific design of the waveguide and resonators, $g/2\pi$ can range from a few kHz to more than 10 MHz.

Note that we can engineer the coupling rate by tailoring or shaping the contact area between the waveguide and the resonator.

C. Isolating intra-node spin-mechanical coupling from the waveguides

We separate the spin qubits in a spin-mechanical resonator into logic qubits and communication qubits, which are used exclusively for quantum state transfer between neighboring quantum nodes. Ideally, intra-node interactions should be decoupled from the phononic waveguides, since residual coupling of the logic qubits to the adjacent waveguides leads to additional decoherence.

The band gaps of the phononic crystal waveguides can be exploited to isolate the intranode spin-mechanical coupling from the waveguides. Specifically, the logic qubits can couple to each other and to the communication qubits through a resonator mode with a frequency that is in the band gap of both phononic crystal waveguides, i.e. in the overlapping spectral region of the two phononic band gaps, as highlighted by the yellow shaded area in Fig. 3b. In this case, the phonon-mediated coupling among the logic qubits and the communication qubits within a spinmechanical resonator or a quantum node is decoupled from the adjacent waveguides. For the resonator-waveguide design shown in Fig. 3a, the fourth order compressional mode of the resonator, with ω_R =1.3258 GHz, falls in the band gap of both phononic crystal waveguides and can thus serve as a mechanical mode for intra-node spin-mechanical coupling. Other resonator modes in the overlapping region of the two band gaps can also be used for this purpose, providing flexibility in the physical location of the logic qubits.

D. Protecting phononic networks with a 2D phononic crystal lattice

To protect the relevant mechanical modes from the surrounding mechanical environment, we embed the entire phononic network in a 2D phononic crystal lattice, as illustrated in Fig. 4. 2D phononic crystal lattices have been used extensively in earlier studies to isolate mechanical systems such as optomechanical crystals, membranes, and single-mode phononic wires from the surrounding environment [61-63]. The use of 2D phononic crystal shields has led to the experimental realization of ultrahigh mechanical Q-factors, with $\omega Q_m/2\pi$ approaching or even exceeding 10^{17} [64,65].

Figure 4b plots the phononic band structure of the symmetric mechanical modes in the 2D phononic crystal lattice shown in Fig. 4a. The band structure of the 2D lattice features a band gap between 0.85 and 2.25 GHz, spanning the phononic band gaps of both phononic crystal waveguides A and B and thus protecting all the mechanical modes relevant to the phononic quantum network. For the design shown in Fig. 4a, only waveguide B is attached to the 2D lattice, because this waveguide and the 2D square lattice have the same period. In this case, mechanical modes with frequencies near ω_A are isolated from the environment by the band gap in the 2D lattice as well as the band gap in waveguide B, which also relaxes the requirement that the band gap of the 2D lattice spans both ω_A and ω_B .

The specific design for the mechanical resonators, phononic crystal waveguides, and 2D phononic crystal shields discussed in this section is by no means optimal. The design serves as an example for implementing the proposed network architecture in a phononic network.

III. QUANTUM STATE TRANSFERS

Mechanically-mediated quantum state transfers have been investigated theoretically for optomechanical transducers that can interface hybrid quantum systems[66-71]. State transfer processes that can be robust against thermal mechanical noise have also been proposed. One approach is based on the use of dark modes, which are decoupled from the relevant mechanical system through destructive interference[72,73]. Dark modes in multimode optomechanical and electromechanical systems have been realized experimentally [74-76]. Another approach returns the mediating mechanical mode to its initial state, disentangling the mechanical mode from the rest of the system[77,78].

The closed mechanical subsystem discussed in Section II (also see Fig. 1b) consists of three mechanical modes, including two resonator modes in the respective mechanical resonators, described by annihilation operators, \hat{a}_1 and \hat{a}_2 , and a waveguide mode, described by \hat{b} . For simplicity, we assume that the two resonator modes couple to the waveguide mode with equal coupling rate g and all three mechanical modes have the same resonance frequency, unless otherwise specified. Each resonator mode couples to either a single spin or an ensemble of spins. For the quantum state transfer between the two spin systems in the respective resonators, the interaction Hamiltonian is given by,

$$H_I = \hbar g \hat{b}^+(\hat{a}_1 + \hat{a}_2) + \hbar [G_1(t)\hat{S}_1\hat{a}_1^+ + G_2(t)\hat{S}_2\hat{a}_2^+] + h.c., \tag{2}$$

where \hat{S}_1 and \hat{S}_2 describe the spin systems, as will be discussed in more detail later, and $G_1(t)$ and $G_2(t)$ are the corresponding spin-mechanical coupling rates. Note that spin qubits in a given resonator can couple to various mechanical modes of the resonator. As discussed in Section II.A, the mode selection for the spin-mechanical coupling is set by the detuning between the external laser driving fields or by the frequency of the microwave driving field.

We assume that the relevant mechanical modes in the two resonators are cooled to their motional ground state. This can be achieved via resolved sideband cooling using a phonon-assisted optical transition[54], along with cryogenic cooling. Because of the protection provided by the 2D phononic crystal shield, the mechanical damping rate, γ , can in principle be much smaller than the relevant coupling rate such that mechanical losses can be ignored during the transfer process. With $G >> k_B T / \hbar Q_m$, the effects of thermal heating during the transfer process can also be negligible. For T=1 K and G on the order of 0.1 MHz, this requires $Q_m >> 10^5$, a regime readily achievable in state-of-the-art phononic nanostructures.

We consider two quantum state transfer schemes based on the use of single spins and spin ensembles, respectively. Both schemes return the waveguide mode to its initial state and are thus independent of the initial state of the waveguide. Since the effects of heating are assumed to be negligible and the schemes are independent of the initial state of the waveguide, we calculate the transfer fidelity at zero temperature and examine other relevant limiting factors.

A. Quantum state transfer between single spins

For the single-spin based transfer scheme, we assume $(G_1, G_2) >> g$. The spin operator in Eq. (2) corresponds to the lowering operator for a single spin, with $\hat{S} = \hat{\sigma} = |-> <+|$. The single spin, which serves as a communication qubit, can be positioned near the node of the resonator mode, where the spin-mechanical coupling reaches its maximum value. For the resonant Raman process shown in Fig. 2b, the effective spin-mechanical coupling rate for a single spin is given by $G = g_s \Omega_+ \Omega_- / (4 | \Delta_+ | \omega_m)$ [52]. With estimated D=5 eV and x_{zpf} =0.75x10⁻¹⁵ m, we have $G/2\pi$ =0.1 MHz, where we take $\Omega_+/2\pi = \Omega_-/2\pi$ =0.6 GHz, $\Delta_+/2\pi = 3$ GHz, and $\omega_m/2\pi$ =1 GHz.

As shown in Fig. 5, the state transfer between the two spin systems can take place in a simple triple-swap process. For the first swap, we set $G_2=0$ and turn on G_1 for a duration $\tau_1=\pi/2G_1$, mapping the spin state for \hat{S}_1 to the state for \hat{a}_1 . For the second swap, we set $G_1=G_2=0$. After a duration $\tau_2=\pi/\sqrt{2}g$, the state of \hat{a}_1 is effectively mapped to that of \hat{a}_2 [78]. This waveguide-mediated mapping between the two mechanical resonators leaves the state in the waveguide unchanged, as shown in Fig. 5. For the third swap, we set $G_1=0$ and turn on G_2 for a duration $\tau_3=\pi/2G_2$, mapping the state from \hat{a}_2 to \hat{S}_2 .

The unavoidable coupling to the waveguide mode during the swaps between the single spin and the resonator modes (i.e. the first and the third swap) limits the fidelity of the overall quantum state transfer, which is defined as $\mathcal{F} = \left(\operatorname{Tr} \left[\left(\sqrt{\rho(t_i)} \rho(t_f) \sqrt{\rho(t_i)} \right)^{1/2} \right]^2 \right]^2$ [79]. Figure 6a shows the fidelity, with the initial state given by $|\psi(t_i)>=|+>|->|0,0,0>$, as a function of G/g where G is the peak value for both G_1 and G_2 . High fidelity can be achieved only when G/g>>1, which is difficult to achieve experimentally. Figure 6b also plots the fidelity when the duration of the $\pi/2$ pulses deviates from the ideal value. For relatively small G/g, the maximum fidelity actually occurs away from the zero deviation, $\varepsilon=0$. This is because for the phononic network, g is a constant. The mechanical resonators remain coupled to the waveguide in the first and the third swap of the state transfer process. In the limit that G/g>>1, the maximum fidelity occurs at $\varepsilon=0$, as shown in Fig. 6b.

Detuning between the individual mechanical modes can also limit the fidelity of the state transfer. Here we can assume that the single spin couples resonantly to the respective resonator mode since the corresponding detuning is set by the frequency of the driving lasers. Figure 6c shows the fidelity as a function of the detuning, δ , between the waveguide and the two resonator modes (which are assumed to have equal frequency). As expected, high fidelity is achieved when the detuning is small compared with g.

B. Quantum state transfer between spin ensembles

For the spin-ensemble based transfer scheme, the spin operator in Eq. (2) corresponds to the collective lowering operator for a spin ensemble, with

$$\hat{S} = \frac{1}{\sqrt{\langle \sum_{m} (|-\rangle \langle -|-|+\rangle \langle +|)_{m} \rangle}} \sum_{m} \hat{\sigma}_{m}.$$
 (3)

Ground-state spin-strain coupling of SiV or GeV centers can be used to avoid large optical inhomogeneous broadening of the NV centers. Alternatively, a relatively large optical dipole detuning, Δ , can be used for the ensemble NV centers. For sufficiently weak coupling of individual spins, we can approximate \hat{S} as a bosonic operator, with $[\hat{S}, \hat{S}^+]=1$. Similar approximations for spin ensembles have also been used for thermally-robust quantum state transfer in an optical network[11,12]. In this limit, the overall system can be approximated as a set of linearly coupled harmonic oscillators.

With $G_1=G_2=G$, the interaction Hamiltonian can be written in terms of super modes, with $\hat{a}_{\pm}=(\hat{a}_1\pm\hat{a}_2)/\sqrt{2}$ and $\hat{S}_{\pm}=(\hat{S}_1\pm\hat{S}_2)/\sqrt{2}$, and with the form

$$H_I = \sqrt{2}\hbar g \hat{b}^+ \hat{a}_+ + \hbar G(\hat{S}_+^+ \hat{a}_+ + \hat{S}_-^+ \hat{a}_-) + h.c..$$
 (4)

The corresponding Heisenberg equations can be solved analytically. The time evolution of \hat{S}_1 is given by

$$\hat{S}_{1}(t) = \frac{gG}{\Gamma^{2}} [\cos(\Gamma t) - 1] \hat{b} - \frac{iG}{\sqrt{2}\Gamma} \sin(\Gamma t) \hat{a}_{+} - \frac{i}{\sqrt{2}} \sin(Gt) \hat{a}_{-} \\
+ \frac{1}{\sqrt{2}} [1 + \frac{G^{2}}{\Gamma^{2}} (\cos(\Gamma t) - 1)] \hat{S}_{+} + \frac{1}{\sqrt{2}} \cos(Gt) \hat{S}_{-} \tag{5}$$

where
$$\Gamma = \sqrt{2g^2 + G^2}$$
.

For the case that $\Gamma = 2nG$, where n is a positive integer, $\hat{S}_1(t = \pi/G) = \hat{S}_2$, as can be seen from Eq. (5), which enables a perfect state transfer between the two spin systems, provided that \hat{S} can be approximated as a bosonic operator. This state transfer process is independent of the initial states of the two mechanical resonators as well as the initial state of the phononic crystal waveguide.

To gain further physical insights into the quantum state transfer process, we plot in Fig. 7 the dynamics of the constituent mechanical and spin-ensemble systems under a constant spin-mechanical coupling. For simplicity, we assume that at t=0, the occupation in \hat{S}_1 , \hat{a}_1 , and \hat{b} is 1 and that in \hat{S}_2 and \hat{a}_2 is 0. As shown in Figs. 7a (with $\Gamma=2G$) and 7b (with $\Gamma=4G$), an effective

 π -pulse (with duration $\tau = \pi/G$) swaps the quantum states of the two spin systems as well as those of the two mechanical resonator modes and returns the waveguide mode to its initial state. Because of the bosonic approximation of the spin ensembles, the dynamics of the constituent mechanical and spin systems are periodic. With $\Gamma = 2nG$, the complete state swapping between the two spin ensembles occurs simultaneously with that between the two mechanical resonator modes. This state swapping process, which arises from the special periodic dynamics of the system, is independent of the phonon occupation or distribution in the individual mechanical modes (waveguide or resonator modes) and keeps the mechanical and the spin systems disentangled. In this regard, the state transfer is robust against the overall thermal environment.

The above state transfer scheme requires a careful tuning of the spin-mechanical coupling rate, G, to satisfy the condition, $\Gamma = 2nG$. Nevertheless, the quantum state transfer process can tolerate considerable deviations of G from its targeted or optimal value. As shown in Fig. 8a, even with a deviation as large as 6%, the fidelity of the state transfer calculated with the effective Hamiltonian given in Eq. (4) can still exceed 0.99 (see the shaded area in Fig. 8a).

In the limit that $\Gamma >> G$ (which implies G << g), the fast dynamics of the "+" super-modes interacting with mode \hat{b} effectively average to zero. As a result, the time evolution of mode \hat{b} have negligible effects on the dynamics of the spin system, as shown in Fig. 7c. In this case, the time evolution can be described by the effective Hamiltonian

$$H_{eff} = \hbar G(\hat{S}_{-}^{+} \hat{a}_{-} + \hat{S}_{-} \hat{a}_{-}^{+}). \tag{6}$$

The complete state swap between the two spin systems can now occur to the zeroth order of the small parameter G/g, with $\hat{S}_1(t=\pi/G)=\hat{S}_2$ and without the requirement that $\Gamma=2nG$.

In the regime of $G \ll g$, spin dephasing induced by the nuclear spin bath becomes a major limiting factor for the quantum state transfer process. Figure 8b shows the fidelity for the state transfer as a function of the spin dephasing time, T_2 *, calculated with the effective Hamiltonian given in Eq. (6) and the corresponding density matrix equations. As expected, high fidelity can only be achieved when $1/T_2$ * is small compared with G. In addition to the use of isotopically purified diamond[80], spin dephasing can also be greatly suppressed with the use of dressed, instead of, bare spin states[81,82].

IV. SUMMARY AND OUTLOOK

In summary, we have developed theoretically a phononic network of solid state spins, in which a given spin-mechanical resonator is coupled to two distinct phononic crystal waveguides. The specially designed band gaps in the alternating waveguides enable bidirectional, but frequency-selective coupling, leading to a new architecture for quantum networks. In this architecture, any two neighboring nodes and the waveguide between them can form a closed subsystem. This conceptually-simple architecture overcomes the inherent obstacles in scaling up phononic quantum networks and avoids the technical difficulty of employing chiral spin-phonon interactions. The proposed phononic quantum network thus provides a promising route for developing quantum computers that can take advantage of robust spin qubits.

We have considered two specific approaches for quantum state transfer between spin systems in neighboring quantum nodes, using single spins and spin ensembles, respectively. An ensemble-spin based protocol, which requires a special ratio between the spin-mechanical and waveguide-resonator coupling rates, can be independent of the initial states of all the mechanical modes involved and thus be robust against the thermal environment. Note that these schemes are intended to illustrate examples of spin-mechanical interactions that can be used for the proposed phononic quantum networks. By using closed subsystems as building blocks, the phononic network can exploit and adopt a variety of quantum state transfer schemes.

While the discussions in this paper use, as a specific example, color centers in diamond, the implementation can be applied or extended to other defect centers or solid-state spin systems such as SiC-based systems[83]. Furthermore, the general architecture and the specific approach of alternating, frequency-selective coupling can be extended to microwave networks of superconducting circuits as well as to photonic networks, and also to 2D quantum networks, for which the implementation of surface codes becomes possible[84].

ACKNOWLEDGEMENTS

This work is supported by AFOSR and by NSF under grants No. 1606227 and No. 1641084.

APPENDIX: MECHANICAL MODES IN DIAMOND PHONONIC STRUCTURES

I. Calculations of normal modes

For wavelengths much larger than the atomic spacing, mechanical modes in an elastic material can be treated as a continuum field with time-dependent displacement at a point \mathbf{r} , given by $\mathbf{Q}(\mathbf{r}, t)$. The field displacement obeys a wave equation

$$\rho \hat{c}_{t}^{2} \mathbf{Q} = (\lambda + \mu) \nabla (\nabla \cdot \mathbf{Q}) + \mu \nabla^{2} \mathbf{Q}. \tag{A1}$$

where ρ is the density of the material. The Lamé constants

$$\lambda = \frac{vE}{(1+v)(1-2v)}, \quad \mu = \frac{E}{2(1+v)}$$
 (A2)

are expressed in terms of the Young's modulus E and Poisson ratio v.

We determine the frequencies and field patterns of the normal modes by solving the corresponding eigenvalue equations using finite element numerical calculations. The material properties of diamond used are E = 1050 GPa, v=0.2, and $\rho = 3539$ kg/m³. All structures under study have mirror symmetries, as illustrated in Fig. A1. The solutions of the wave equations will thus be eigenmodes of the symmetry operations. We organize the solutions as even or odd under reflection R_j about a plane perpendicular to the coordinate axis j = x, y, z. The specific symmetries of the structure are R_y and R_z . All modes considered in this work have even symmetry under R_z . Figure A1 shows the displacement patterns of the third and fourth order compression modes of the thin diamond plate discussed in Fig. 2 of the main text.

II. Resonator-waveguide Coupling Rates

We describe the coupling between the plate resonators and the phononic crystal waveguides by using a standard coupled-mode theory. The Hamiltonian for a pair of single-mode resonators connected by a waveguide is taken to be

$$H = \sum_{n} \hbar \left\{ \Delta_{n} \hat{b}_{n}^{\dagger} \hat{b}_{n} + g_{n} \left[\left(\hat{a}_{1} + (-1)^{n} \hat{a}_{2} \right) \hat{b}_{n}^{\dagger} + h.c. \right] \right\}, \tag{A3}$$

written in a frame rotating at the resonator frequency, where \hat{a}_1 and \hat{a}_2 describe the two resonator modes with the same frequency, \hat{b}_n describes the waveguide modes, g_n is the resonator-waveguide coupling rate, and Δ_n is the frequency difference between the waveguide and the resonator modes. The sign difference on alternating modes reflects alternating symmetry of the eigenmodes in the

waveguide. For a waveguide of length $L = 120 \mu m$, numerical simulations of the diamond waveguide structure used in this study give a mode spacing about 30 MHz. In the limit that g is much less than the mode spacing, only the resonant or nearly resonant waveguide mode \hat{b}_0 needs to be considered.

In the limit of a single waveguide mode, the (unnormalized) eigenmodes are $\psi_0 = a_1 - a_2$ and $\psi_{\pm} = 4gb_0 + (\Delta_0 \pm \Lambda)(a_1 + a_2)$, with corresponding eigenvalues $\lambda_0 = 0$, $\lambda_{\pm} = \frac{1}{2}(\Delta_0 \pm \Lambda)$, where $\Lambda = \sqrt{\Delta_0^2 + 8g^2}$. To determine the relevant resonator-waveguide coupling rates for the phononic network structure, we first calculate numerically the relevant eigenmodes of the full structure. As shown in Fig. A2, the eigenmodes occur as triplets, which arise from the coupling between the unperturbed resonator and waveguide modes. From the frequencies of the given triplet, we can then determine both g and Δ_0 , with

$$\Delta_0 = \lambda_{\perp} + \lambda_{-} - 2\lambda_0, \tag{A4}$$

and

$$g = \sqrt{\frac{(\lambda_{+} - \lambda_{-})^{2} - \Delta_{0}^{2}}{8}}.$$
 (A5)

For the dimensions of the phononic network used in the main text, the third order compression mode features g = 9.0 MHz and $\Delta_0 = -3.4 \text{MHz}$, while the fifth order compression mode features g = 3.1 MHz and $\Delta_0 = -1.9 \text{MHz}$. Further fine tuning of the resonator dimensions can reduce Δ_0 to be much smaller than g. The coupling rate can also be tuned or tailored by shaping the contact area between the plate resonator and the phononic crystal waveguide.

In the single-waveguide-mode limit, the eigenmode ψ_0 should have no contribution from the waveguide mode. As can been seen from the displacement patterns shown in Fig. A2, there are still discernable contributions from the waveguide, which arise from the coupling of the resonators to the adjacent waveguide modes such as $b_{\pm 1}$. In order to avoid the coupling to multiple waveguide modes, the waveguide mode spacing needs to far exceed the waveguide-resonator coupling rate, which puts a limit on both the magnitude of g and the length of the waveguide. In the limit of long waveguides with g much greater than the mode spacing, quantum state transfer schemes similar to those proposed for optical networks can be used[11,12]. For diamond-based phononic network, relatively short waveguides are preferred.

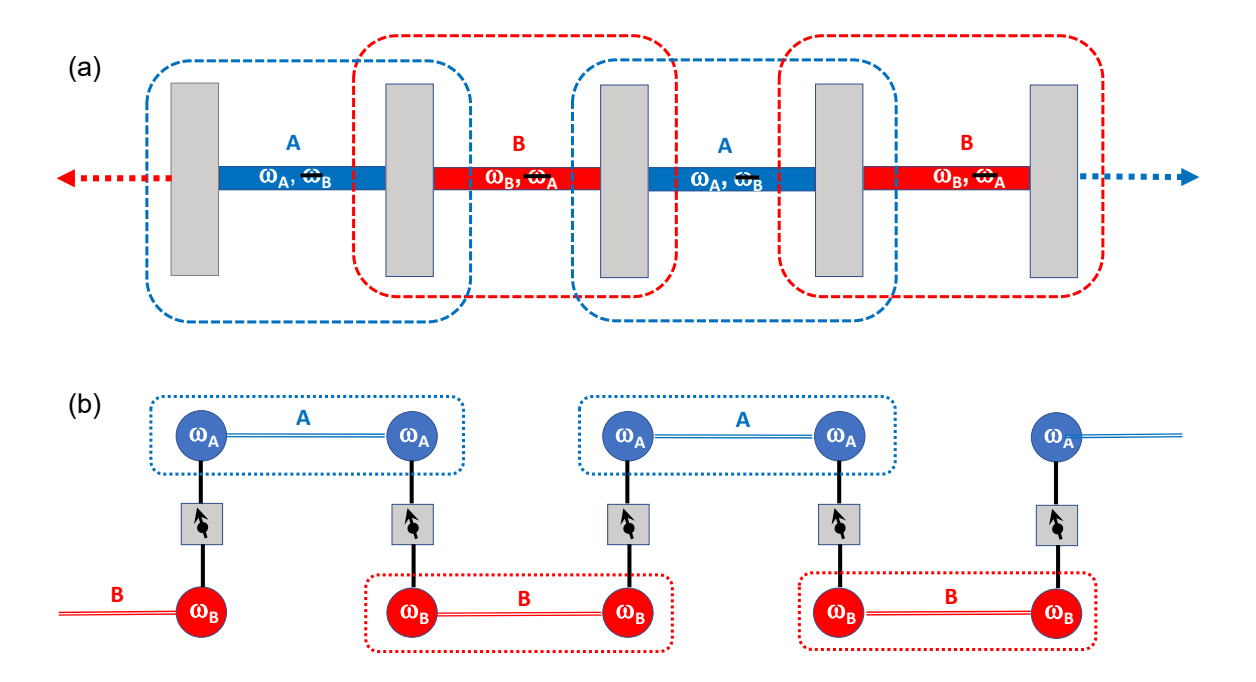


FIG 1. (a) Schematic of a quantum network with alternating and frequency-selective waveguides, in which each quantum node couples to two different waveguides, A and B. Propagation near frequencies ω_A and ω_B is allowed and that near frequencies ω_B and ω_A is forbidden for waveguides A and B, respectively. As indicated by the dashed-line boxes, any two neighboring quantum nodes and the waveguide between them can form a closed subsystem. (b) An implementation using solid state spins and mechanical resonators. In each quantum node, a spin system couples selectively to two resonator modes with frequency ω_A and ω_B . The network consists of closed mechanical subsystems coupled together via the spins.

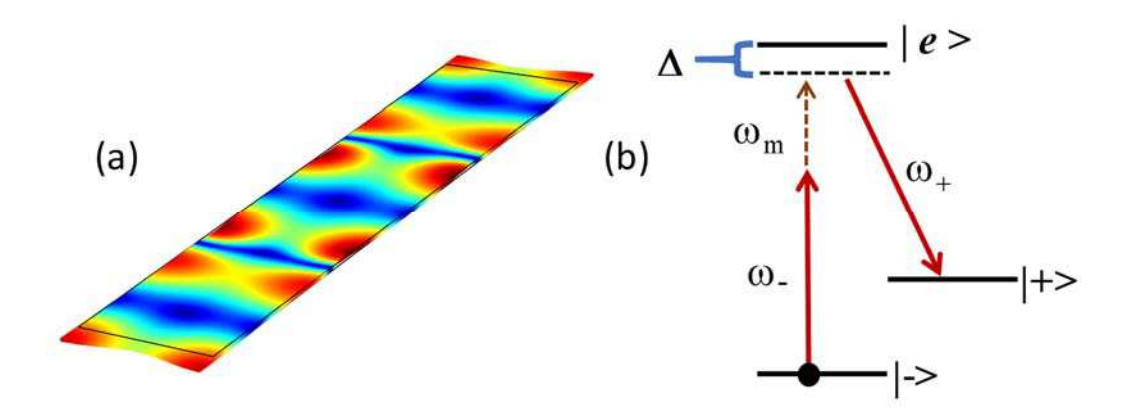


FIG 2. (a) Displacement pattern of a fifth order compression mode in a thin rectangular diamond plate with dimension (27, 8, 0.3) μm . (b) Schematic of a spin qubit coupling to a mechanical mode with frequency ω_m through a resonant Raman process, driven by two external optical fields with frequency ω_+ and ω_- . We can couple the spin qubit to a given mechanical mode by choosing a suitable detuning between ω_+ and ω_- .

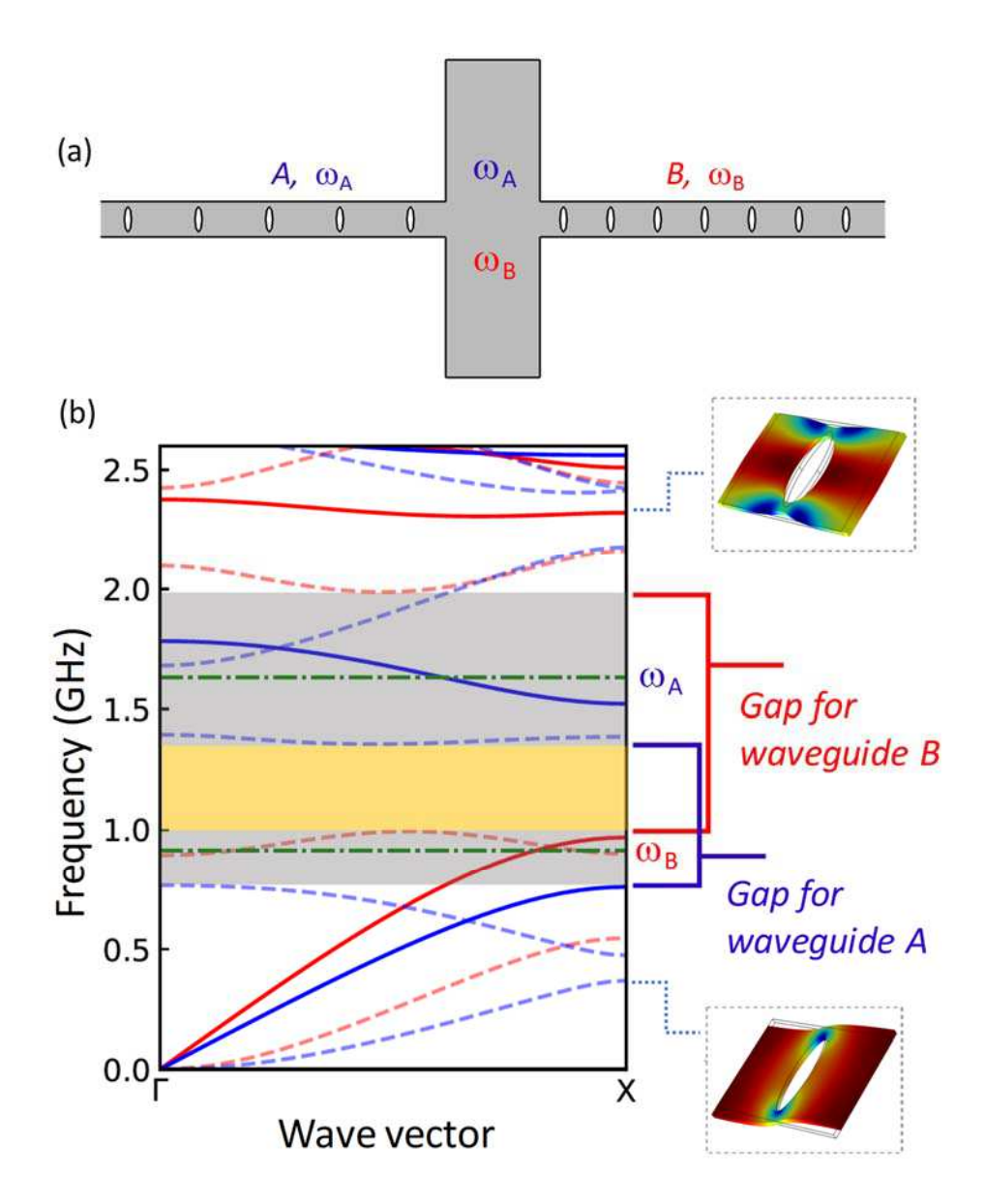


FIG 3. (a) A mechanical resonator couples to two photonic crystal waveguides with a width of 3 μ m and a period of 6 μ m (waveguide A) and 4 μ m (waveguide B). For the elliptical holes in the waveguides, the minor (major) axes are 0.6 (2.2) μ m. (b) Phononic band structures of the two waveguides. Each features a band gap. Blue lines: Waveguide A. Red lines: Waveguide B. The grey shaded areas show non-overlapping regions of the two band gaps. The yellow shaded area shows the overlapping region. Solid (dashed) lines are for modes with displacement patterns that are symmetric (antisymmetric) about the plane that bisects and is normal to both the waveguide and the resonators. Dot-dashed lines indicate the frequencies of the two resonator modes, ω_A and ω_B , used to couple to the respective waveguide modes.

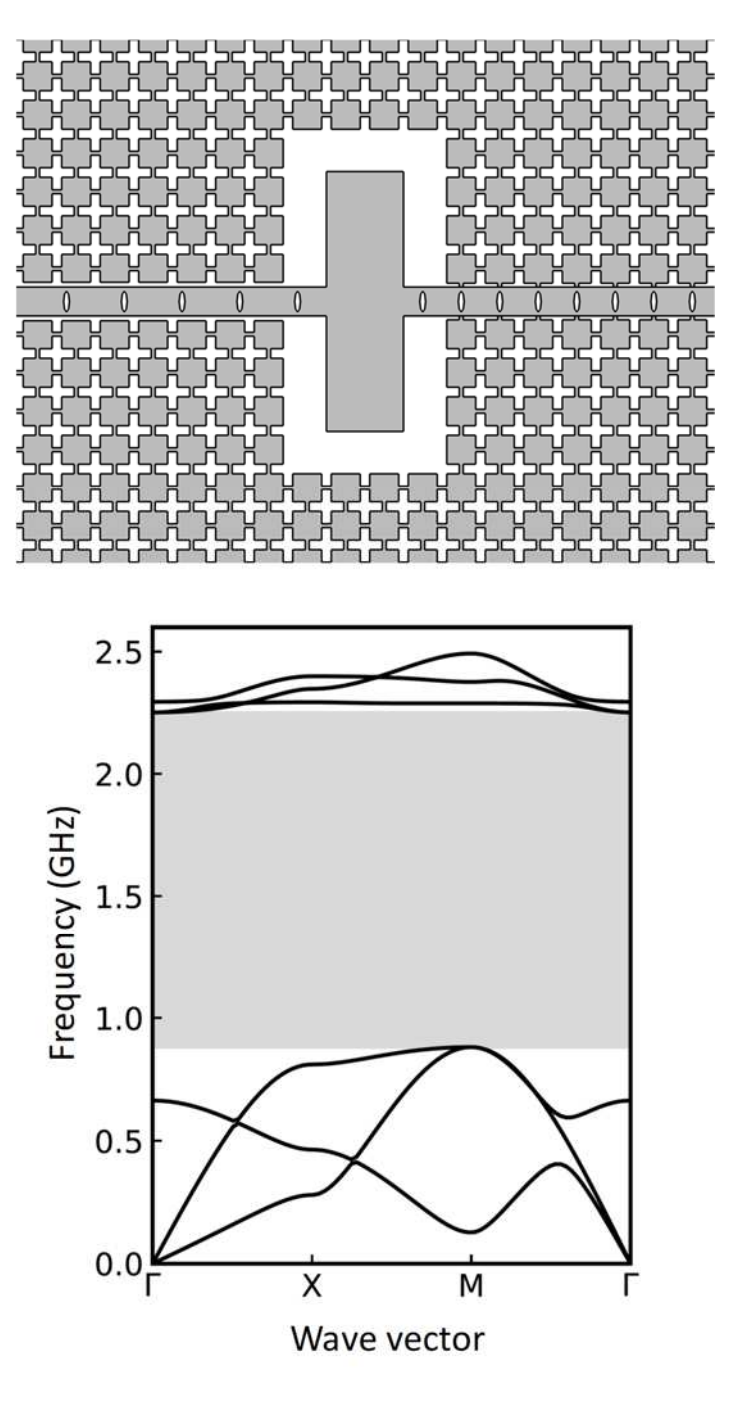


FIG 4. Top: A phononic network embedded in a square photonic crystal lattice with a period of 4 μm . The side length of the squares is 3 μm . The connecting bridges have a length of 1 μm and width of 0.4 μm . Bottom: Phononic band structure of the 2D lattice. Only symmetric modes are shown.

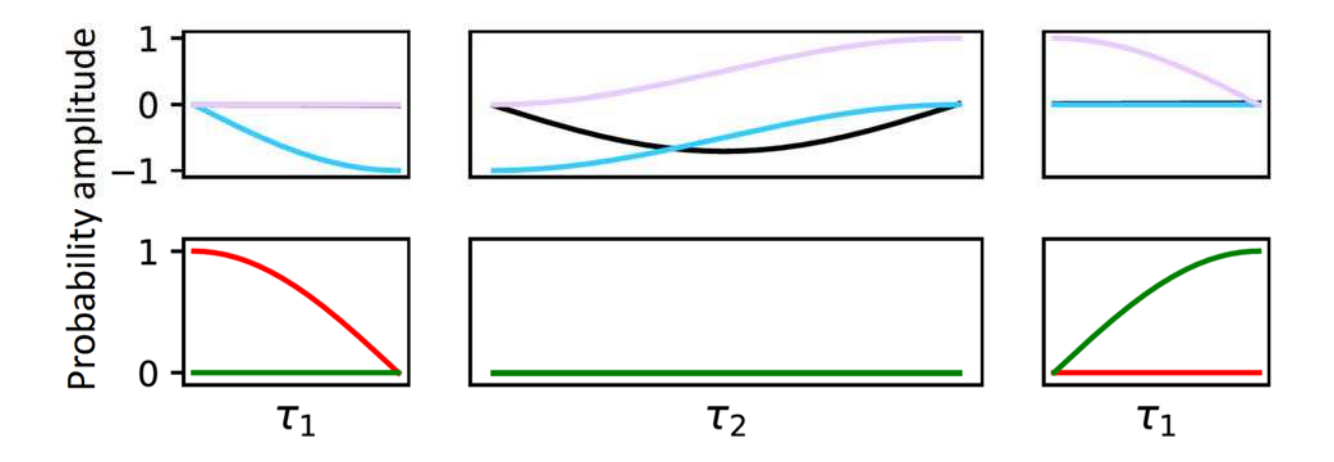


FIG 5. Time evolution of the mechanical and spin systems with G/g = 100 during the three successive swaps, with the same peak value G both G_1 and G_2 . Top: resonator mode 1 (blue), resonator mode 2 (purple), and waveguide mode (black). Bottom: spin 1 (red) and spin 2 (green).

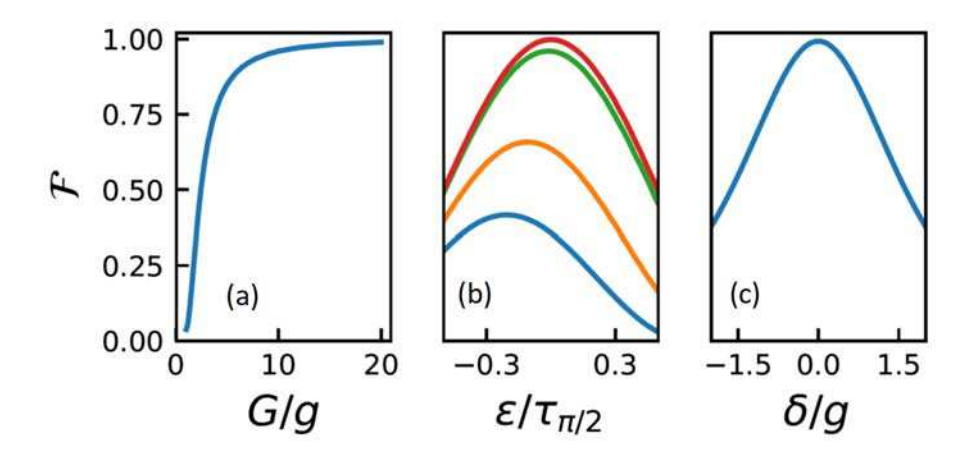


FIG 6. Fidelity for the triple-swap quantum state transfer with an initial state |+>|->|0, 0, 0>. (a) As a function of G/g. (b) As a function of the deviation from the $\pi/2$ pulses. From top to bottom, G/g=50, 10, 3, 2. (c) As a function of the detuning between the waveguide and the two resonator modes, with G/g=25. Ideal pulse duration and detuning are used unless otherwise specified. No other decoherence processes are included.

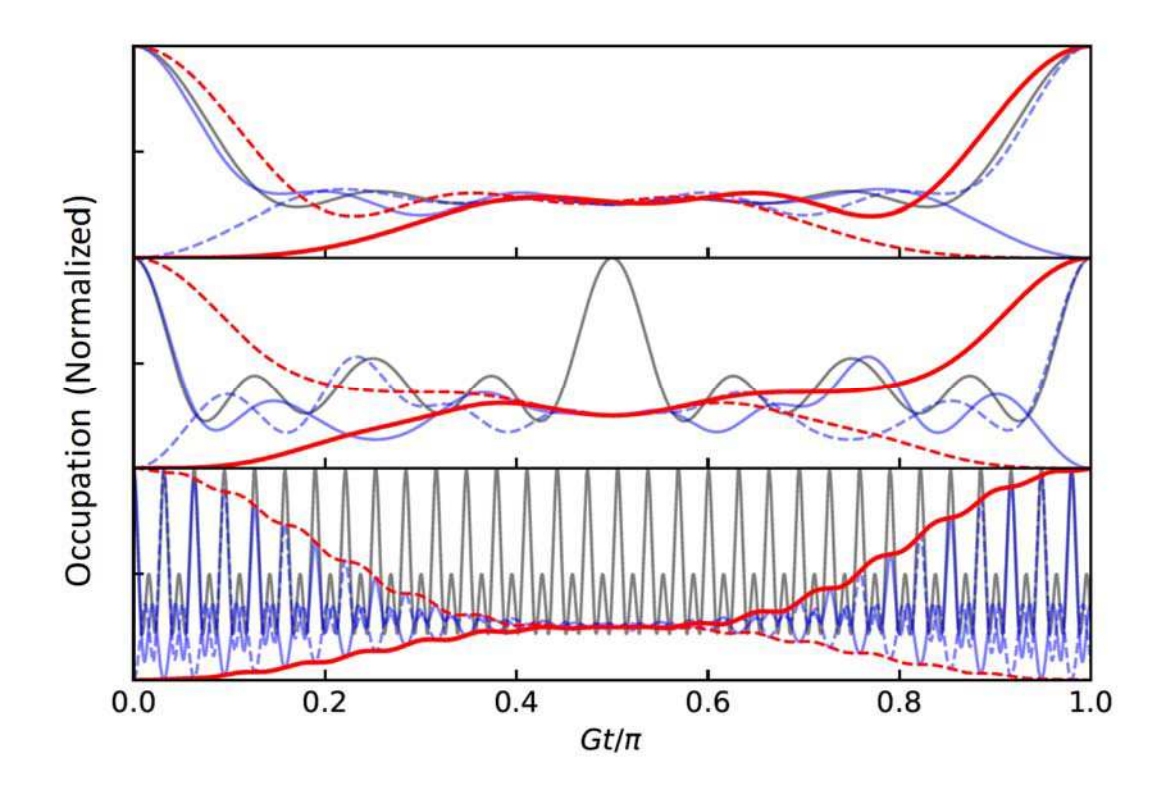


FIG 7. Time evolution of the mechanical and spin-ensemble systems under a constant spin-mechanical coupling, with the initial states specified in the text. Red lines: two spin ensembles. Blue lines: two resonator modes. Grey line: the waveguide mode. Top panel: $\Gamma/G=2$. Middle panel: $\Gamma/G=4$. Bottom panel: $\Gamma/G=\sqrt{1001}$. For both the top and middle panels, the complete state swap between the spin ensembles is accompanied by that between the resonator modes.

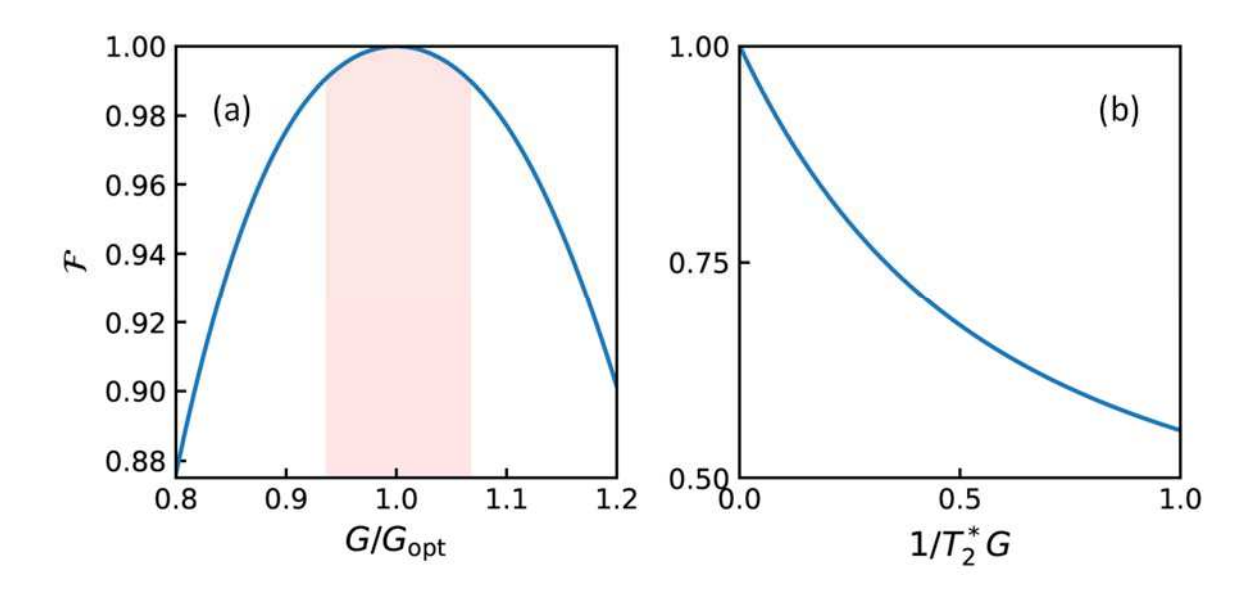


FIG 8. (a) Fidelity of the spin-ensemble based quantum state transfer as a function of G, with Γ/G_{opt} =4 and with the initial states being the same as those used for Fig. 7. No decoherence processes are included. (b) Fidelity of the spin-ensemble based quantum state transfer as a function of the spin dephasing rate, with $G \ll g$ and spin lifetime=10000/G. The fidelity is averaged over all possible initial states. No other decoherence processes are included.

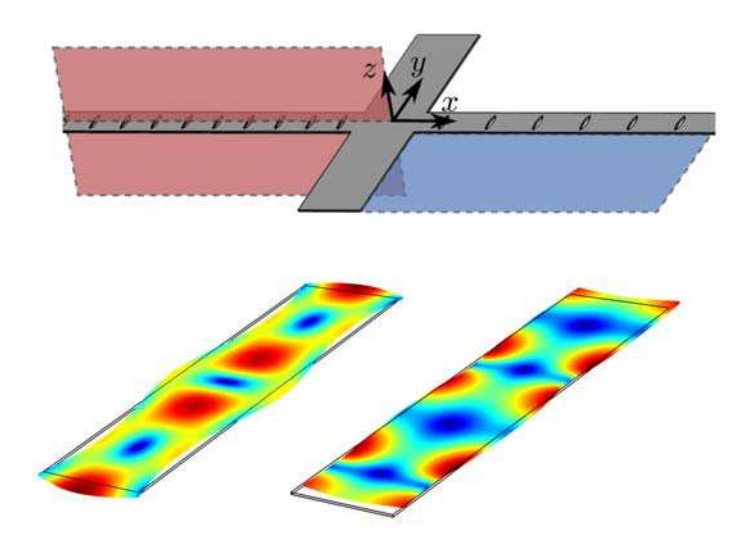


FIG A1. Top: The reflection symmetry planes of the phononic network structure. The blue and red planes correspond to R_z and R_y , respectively. Bottom: Displacement patterns of the third order compression mode (left), with even R_y symmetry, and fourth order compression mode (right), with odd R_y symmetry.

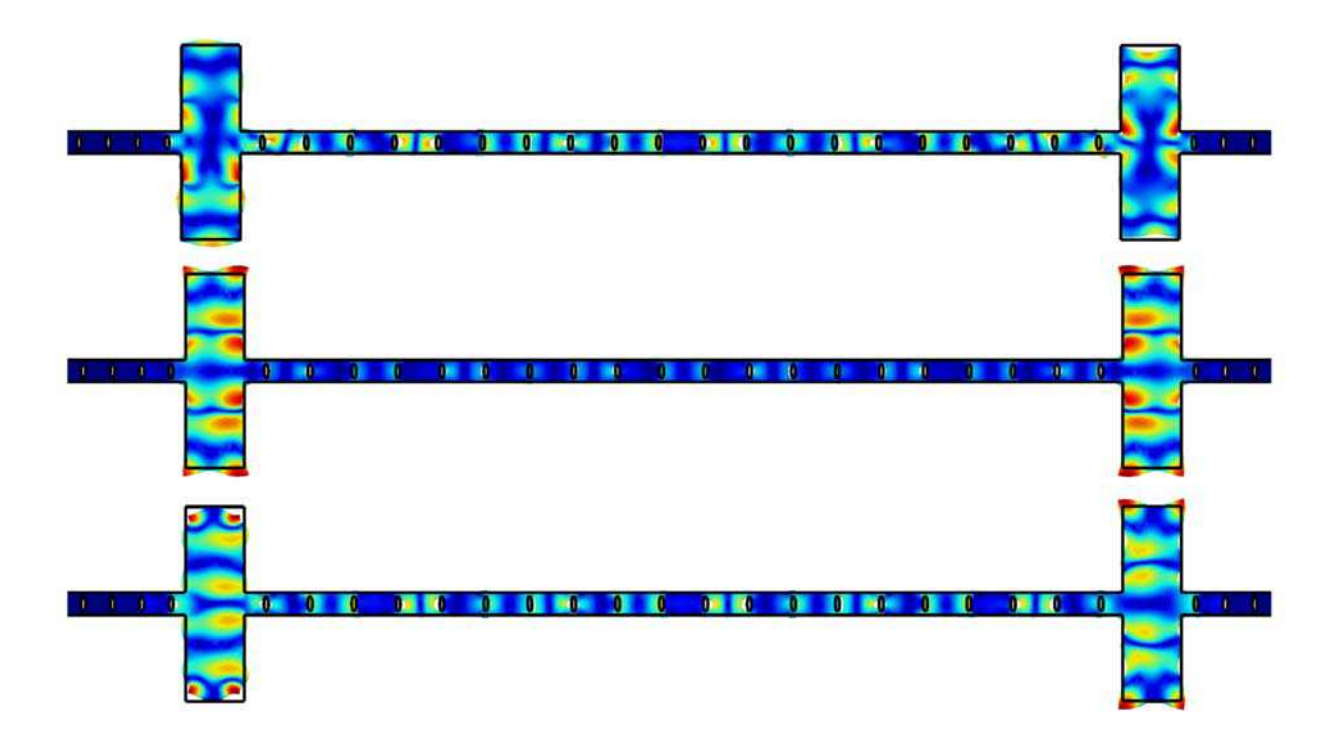


FIG A2: Displacement patterns of three eigenmodes of the phononic network structure shown in Fig. 3 of the main text. The frequencies are $(1.6737,\,1.6791,\,1.6826)$ GHz from top to bottom. The triplet arises from the coupling between the fifth order compression modes in the two neighboring plate resonators and the nearly resonant waveguide mode. The array of holes in the waveguide has a period of 6 μ m.

REFERENCES:

- [1] H. J. Kimble, *The quantum internet*, Nature **453**, 1023 (2008).
- [2] K. Hammerer, A. S. Sorensen, and E. S. Polzik, *Quantum interface between light and atomic ensembles*, Reviews of Modern Physics **82**, 1041 (2010).
- [3] L. M. Duan and C. Monroe, *Colloquium: Quantum networks with trapped ions*, Reviews of Modern Physics **82**, 1209 (2010).
- [4] T. E. Northup and R. Blatt, *Quantum information transfer using photons*, Nature Photonics **8**, 356 (2014).
- [5] A. Reiserer and G. Rempe, *Cavity-based quantum networks with single atoms and optical photons*, Reviews of Modern Physics **87**, 1379 (2015).
- [6] S. J. M. Habraken, K. Stannigel, M. D. Lukin, P. Zoller, and P. Rabl, *Continuous mode cooling and phonon routers for phononic quantum networks*, New Journal of Physics **14**, 115004 (2012).
- [7] M. V. Gustafsson, T. Aref, A. F. Kockum, M. K. Ekstrom, G. Johansson, and P. Delsing, *Propagating phonons coupled to an artificial atom*, Science **346**, 207 (2014).
- [8] M. J. A. Schuetz, E. M. Kessler, G. Giedke, L. M. K. Vandersypen, M. D. Lukin, and J. I. Cirac, *Universal Quantum Transducers Based on Surface Acoustic Waves*, Physical Review X 5, 031031 (2015).
- [9] J. I. Cirac, P. Zoller, H. J. Kimble, and H. Mabuchi, *Quantum state transfer and entanglement distribution among distant nodes in a quantum network*, Phys. Rev. Lett. **78**, 3221 (1997).
- [10] H. J. Carmichael, *Quantum Trajectory Theory for Cascaded Open Systems*, Physical Review Letters **70**, 2273 (1993).
- [11] B. Vermersch, P. O. Guimond, H. Pichler, and P. Zoller, *Quantum State Transfer via Noisy Photonic and Phononic Waveguides*, Physical Review Letters **118**, 133601 (2017).
- [12] Z. L. Xiang, M. Z. Zhang, L. Jiang, and P. Rabl, *Intracity Quantum Communication via Thermal Microwave Networks*, Physical Review X 7, 011035 (2017).
- [13] K. Y. Bliokh, F. J. Rodriguez-Fortuno, F. Nori, and A. V. Zayats, *Spin-orbit interactions of light*, Nature Photonics **9**, 796 (2015).
- [14] P. Lodahl, S. Mahmoodian, S. Stobbe, A. Rauschenbeutel, P. Schneeweiss, J. Volz, H. Pichler, and P. Zoller, *Chiral quantum optics*, Nature **541**, 473 (2017).
- [15] R. Mitsch, C. Sayrin, B. Albrecht, P. Schneeweiss, and A. Rauschenbeutel, *Quantum state-controlled directional spontaneous emission of photons into a nanophotonic waveguide*, Nature Communications 5, 5713 (2014).
- [16] I. Sollner, S. Mahmoodian, S. L. Hansen, L. Midolo, A. Javadi, G. Kirsanske, T. Pregnolato, H. El-Ella, E. H. Lee, J. D. Song, S. Stobbe, and P. Lodahl, *Deterministic photon-emitter coupling in chiral photonic circuits*, Nature Nanotechnology **10**, 775 (2015).
- [17] M.-A. Lemonde, S. Meesala, A. Sipahigil, M. J. A. Schuetz, M. D. Lukin, M. Loncar, and P. Rabl, *Phonon networks with SiV centers in diamond waveguides*, arXiv:1801.01904 (2018).
- [18] C. Monroe and J. Kim, Scaling the Ion Trap Quantum Processor, Science 339, 1164 (2013).
- [19] D. A. Golter, T. Oo, M. Amezcua, K. A. Stewart, and H. L. Wang, *Optomechanical Quantum Control of a Nitrogen-Vacancy Center in Diamond*, Physical Review Letters **116**, 143602 (2016).
- [20] D. Hatanaka, I. Mahboob, K. Onomitsu, and H. Yamaguchi, *Phonon waveguides for electromechanical circuits*, Nature Nanotechnology **9**, 520 (2014).
- [21] A. Sipahigil, R. E. Evans, D. D. Sukachev, M. J. Burek, J. Borregaard, M. K. Bhaskar, C. T. Nguyen, J. L. Pacheco, H. A. Atikian, C. Meuwly, R. M. Camacho, F. Jelezko, E. Bielejec, H. Park, M. Loncar, and M. D. Lukin, *An integrated diamond nanophotonics platform for quantum-optical networks*, Science **354**, 847 (2016).
- [22] M. J. Burek, J. D. Cohen, S. M. Meenehan, N. El-Sawah, C. Chia, T. Ruelle, S. Meesala, J. Rochman, H. A. Atikian, M. Markham, D. J. Twitchen, M. D. Lukin, O. Painter, and M. Loncar, *Diamond optomechanical crystals*, Optica **3**, 1404 (2016).
- [23] N. H. Wan, S. Mouradian, and D. Englund, *Two-Dimensional Photonic Crystal Slab Nanocavities on Bulk Single-Crystal Diamond*, arXiv preprint arXiv:1801.01151 (2008).

- [24] M. W. Doherty, N. B. Manson, P. Delaney, F. Jelezko, J. Wrachtrup, and L. C. L. Hollenberg, *The nitrogen-vacancy colour centre in diamond*, Phys Rep **528**, 1 (2013).
- [25] D. D. Awschalom, L. C. Bassett, A. S. Dzurak, E. L. Hu, and J. R. Petta, *Quantum Spintronics: Engineering and Manipulating Atom-Like Spins in Semiconductors*, Science **339**, 1174 (2013).
- [26] L. Childress, R. Walsworth, and M. Lukin, *Atom-like crystal defects: From quantum computers to biological sensors*, Phys Today **67**, 38 (2014).
- [27] F. Jelezko, T. Gaebel, I. Popa, A. Gruber, and J. Wrachtrup, *Observation of coherent oscillations in a single electron spin*, Physical Review Letters **92**, 076401 (2004).
- [28] L. Childress, M. V. G. Dutt, J. M. Taylor, A. S. Zibrov, F. Jelezko, J. Wrachtrup, P. R. Hemmer, and M. D. Lukin, *Coherent dynamics of coupled electron and nuclear spin qubits in diamond*, Science **314**, 281 (2006).
- [29] G. D. Fuchs, V. V. Dobrovitski, D. M. Toyli, F. J. Heremans, and D. D. Awschalom, *Gigahertz Dynamics of a Strongly Driven Single Quantum Spin*, Science **326**, 1520 (2009).
- [30] G. de Lange, Z. H. Wang, D. Riste, V. V. Dobrovitski, and R. Hanson, *Universal Dynamical Decoupling of a Single Solid-State Spin from a Spin Bath*, Science **330**, 60 (2010).
- [31] C. G. Yale, B. B. Buckley, D. J. Christle, G. Burkard, F. J. Heremans, L. C. Bassett, and D. D. Awschalom, *All-optical control of a solid-state spin using coherent dark states*, Proceedings of the National Academy of Sciences of the United States of America **110**, 7595 (2013).
- [32] D. A. Golter and H. L. Wang, *Optically Driven Rabi Oscillations and Adiabatic Passage of Single Electron Spins in Diamond*, Physical Review Letters **112**, 116403 (2014).
- [33] L. C. Bassett, F. J. Heremans, D. J. Christle, C. G. Yale, G. Burkard, B. B. Buckley, and D. D. Awschalom, *Ultrafast optical control of orbital and spin dynamics in a solid-state defect*, Science **345**, 1333 (2014).
- [34] S. D. Barrett and P. Kok, Efficient high-fidelity quantum computation using matter qubits and linear optics, Physical Review A 71, 060310(R) (2005).
- [35] Q. Chen, W. L. Yang, M. Feng, and J. F. Du, *Entangling separate nitrogen-vacancy centers in a scalable fashion via coupling to microtoroidal resonators*, Physical Review A **83**, 054305 (2011).
- [36] K. Nemoto, M. Trupke, S. J. Devitt, A. M. Stephens, B. Scharfenberger, K. Buczak, T. Nobauer, M. S. Everitt, J. Schmiedmayer, and W. J. Munro, *Photonic Architecture for Scalable Quantum Information Processing in Diamond*, Physical Review X **4**, 031022 (2014).
- [37] A. Sipahigil, K. D. Jahnke, L. J. Rogers, T. Teraji, J. Isoya, A. S. Zibrov, F. Jelezko, and M. D. Lukin, *Indistinguishable Photons from Separated Silicon-Vacancy Centers in Diamond*, Physical Review Letters **113**, 113602 (2014).
- [38] L. J. Rogers, K. D. Jahnke, T. Teraji, L. Marseglia, C. Muller, B. Naydenov, H. Schauffert, C. Kranz, J. Isoya, L. P. McGuinness, and F. Jelezko, *Multiple intrinsically identical single-photon emitters in the solid state*, Nature Communications **5**, 4739 (2014).
- [39] M. K. Bhaskar, D. D. Sukachev, A. Sipahigil, R. E. Evans, M. J. Burek, C. T. Nguyen, L. J. Rogers, P. Siyushev, M. H. Metsch, H. Park, F. Jelezko, M. Loncar, and M. D. Lukin, *Quantum Nonlinear Optics with a Germanium-Vacancy Color Center in a Nanoscale Diamond Waveguide*, Physical Review Letters 118, 223603 (2017).
- [40] P. Siyushev, M. H. Metsch, A. Ijaz, J. M. Binder, M. K. Bhaskar, D. D. Sukachev, A. Sipahigil, R. E. Evans, C. T. Nguyen, M. D. Lukin, P. R. Hemmer, Y. N. Palyanov, I. N. Kupriyanov, Y. M. Borzdov, L. J. Rogers, and F. Jelezko, *Optical and microwave control of germanium-vacancy center spins in diamond*, Physical Review B **96**, 081201(R) (2017).
- [41] Y. Chu, N. P. de Leon, B. J. Shields, B. Hausmann, R. Evans, E. Togan, M. J. Burek, M. Markham, A. Stacey, A. S. Zibrov, A. Yacoby, D. J. Twitchen, M. Loncar, H. Park, P. Maletinsky, and M. D. Lukin, *Coherent Optical Transitions in Implanted Nitrogen Vacancy Centers*, Nano Letters **14**, 1982 (2014).
- [42] R. E. Evans, A. Sipahigil, D. D. Sukachev, A. S. Zibrov, and M. D. Lukin, *Narrow-Linewidth Homogeneous Optical Emitters in Diamond Nanostructures via Silicon Ion Implantation*, Phys Rev Appl 5, 044010 (2016).

- [43] O. Arcizet, V. Jacques, A. Siria, P. Poncharal, P. Vincent, and S. Seidelin, *A single nitrogen-vacancy defect coupled to a nanomechanical oscillator*, Nature Physics 7, 879 (2011).
- [44] S. Kolkowitz, A. C. B. Jayich, Q. P. Unterreithmeier, S. D. Bennett, P. Rabl, J. G. E. Harris, and M. D. Lukin, *Coherent Sensing of a Mechanical Resonator with a Single-Spin Qubit*, Science **335**, 1603 (2012).
- [45] E. R. MacQuarrie, T. A. Gosavi, N. R. Jungwirth, S. A. Bhave, and G. D. Fuchs, *Mechanical Spin Control of Nitrogen-Vacancy Centers in Diamond*, Physical Review Letters **111**, 227602 (2013).
- [46] J. Teissier, A. Barfuss, P. Appel, E. Neu, and P. Maletinsky, *Strain Coupling of a Nitrogen-Vacancy Center Spin to a Diamond Mechanical Oscillator*, Physical Review Letters **113**, 020503 (2014).
- [47] P. Ovartchaiyapong, K. W. Lee, B. A. Myers, and A. C. B. Jayich, *Dynamic strain-mediated coupling of a single diamond spin to a mechanical resonator*, Nature Communications **5**, 4429 (2014).
- [48] E. R. MacQuarrie, T. A. Gosavi, S. A. Bhave, and G. D. Fuchs, *Continuous dynamical decoupling of a single diamond nitrogen-vacancy center spin with a mechanical resonator*, Physical Review B **92**, 224419 (2015).
- [49] A. Barfuss, J. Teissier, E. Neu, A. Nunnenkamp, and P. Maletinsky, *Strong mechanical driving of a single electron spin*, Nature Physics 11, 820 (2015).
- [50] E. R. MacQuarrie, T. A. Gosavi, A. M. Moehle, N. R. Jungwirth, S. A. Bhave, and G. D. Fuchs, *Coherent control of a nitrogen-vacancy center spin ensemble with a diamond mechanical resonator*, Optica **2**, 233 (2015).
- [51] S. Meesala, Y. I. Sohn, H. A. Atikian, S. Kim, M. J. Burek, J. T. Choy, and M. Loncar, *Enhanced Strain Coupling of Nitrogen-Vacancy Spins to Nanoscale Diamond Cantilevers*, Phys Rev Appl **5**, 034010 (2016).
- [52] D. A. Golter, T. Oo, M. Amezcua, I. Lekavicius, K. A. Stewart, and H. L. Wang, *Coupling a Surface Acoustic Wave to an Electron Spin in Diamond via a Dark State*, Physical Review X **6**, 041060 (2016).
- [53] K. W. Lee, D. Lee, P. Ovartchaiyapong, J. Minguzzi, J. R. Maze, and A. C. B. Jayich, *Strain Coupling of a Mechanical Resonator to a Single Quantum Emitter in Diamond*, Phys Rev Appl **6**, 034005 (2016).
- [54] K. V. Kepesidis, S. D. Bennett, S. Portolan, M. D. Lukin, and P. Rabl, *Phonon cooling and lasing with nitrogen-vacancy centers in diamond*, Physical Review B **88**, 064105 (2013).
- [55] A. Albrecht, A. Retzker, F. Jelezko, and M. B. Plenio, *Coupling of nitrogen vacancy centres in nanodiamonds by means of phonons*, New Journal of Physics **15**, 083014 (2013).
- [56] S. Meesala, Y.-I. Sohn, B. Pingault, L. Shao, H. A. Atikian, J. Holzgrafe, M. Gundogan, C. Stavrakas, A. Sipahigil, C. Chia, M. J. Burek, M. Zhang, L. Wu, J. L. Pacheco, J. Abraham, E. Bielejec, M. D. Lukin, M. Atature, and M. Loncar, *Strain engineering of the silicon-vacancy center in diamond*, arXiv:1801.09833 (2018).
- [57] E. Togan, Y. Chu, A. S. Trifonov, L. Jiang, J. Maze, L. Childress, M. V. G. Dutt, A. S. Sorensen, P. R. Hemmer, A. S. Zibrov, and M. D. Lukin, *Quantum entanglement between an optical photon and a solid-state spin qubit*, Nature **466**, 730 (2010).
- [58] X. Chen, I. Lizuain, A. Ruschhaupt, D. Guery-Odelin, and J. G. Muga, *Shortcut to Adiabatic Passage in Two- and Three-Level Atoms*, Physical Review Letters **105**, 123003 (2010).
- [59] B. B. Zhou, A. Baksic, H. Ribeiro, C. G. Yale, F. J. Heremans, P. C. Jerger, A. Auer, G. Burkard, A. A. Clerk, and D. D. Awschalom, *Accelerated quantum control using superadiabatic dynamics in a solid-state lambda system*, Nature Physics **13**, 330 (2017).
- [60] H. Ribeiro, A. Baksic, and A. A. Clerk, *Systematic Magnus-Based Approach for Suppressing Leakage and Nonadiabatic Errors in Quantum Dynamics*, Physical Review X 7, 011021 (2017).
- [61] J. Chan, T. P. M. Alegre, A. H. Safavi-Naeini, J. T. Hill, A. Krause, S. Groblacher, M. Aspelmeyer, and O. Painter, *Laser cooling of a nanomechanical oscillator into its quantum ground state*, Nature **478**, 89 (2011).

- [62] P. L. Yu, K. Cicak, N. S. Kampel, Y. Tsaturyan, T. P. Purdy, R. W. Simmonds, and C. A. Regal, *A phononic bandgap shield for high-Q membrane microresonators*, Applied Physics Letters **104**, 023510 (2014).
- [63] R. N. Patel, Z. Wang, W. Jiang, C. J. Sarabalis, J. T. Hill, and A. H. Safavi-Naeini, *A single-mode phononic wire*, arXiv:1711.00847.
- [64] S. M. Meenehan, J. D. Cohen, G. S. MacCabe, F. Marsili, M. D. Shaw, and O. Painter, *Pulsed Excitation Dynamics of an Optomechanical Crystal Resonator near Its Quantum Ground State of Motion*, Phys Rev X 5, 041002 (2015).
- [65] Y. Tsaturyan, A. Barg, E. S. Polzik, and A. Schliesser, *Ultracoherent nanomechanical resonators* via soft clamping and dissipation dilution, Nat Nanotechnol **12**, 776 (2017).
- [66] K. Stannigel, P. Rabl, A. S. Sorensen, P. Zoller, and M. D. Lukin, *Optomechanical Transducers for Long-Distance Quantum Communication*, Physical Review Letters **105**, 220501 (2010).
- [67] L. Tian and H. L. Wang, *Optical wavelength conversion of quantum states with optomechanics*, Physical Review A **82**, 053806 (2010).
- [68] A. H. Safavi-Naeini and O. Painter, *Proposal for an optomechanical traveling wave phonon-photon translator*, New Journal of Physics **13**, 013017 (2011).
- [69] C. A. Regal and K. W. Lehnert, *From cavity electromechanics to cavity optomechanics*, Journal of Physics: Conference Series **264**, 012025 (2011).
- [70] S. Barzanjeh, M. Abdi, G. J. Milburn, P. Tombesi, and D. Vitali, *Reversible Optical-to-Microwave Quantum Interface*, Physical Review Letters **109**, 130503 (2012).
- [71] C. H. Dong, Y. D. Wang, and H. L. Wang, Optomechanical interfaces for hybrid quantum networks, Natl Sci Rev 2, 510 (2015).
- [72] L. Tian, *Adiabatic State Conversion and Pulse Transmission in Optomechanical Systems*, Physical Review Letters **108**, 153604 (2012).
- [73] Y. D. Wang and A. A. Clerk, *Using Interference for High Fidelity Quantum State Transfer in Optomechanics*, Physical Review Letters **108**, 153603 (2012).
- [74] C. Dong, V. Fiore, M. C. Kuzyk, and H. Wang, *Optomechanical dark mode*, Science **338**, 1609 (2012).
- [75] F. Massel, S. U. Cho, J. M. Pirkkalainen, P. J. Hakonen, T. T. Heikkila, and M. A. Sillanpaa, *Multimode circuit optomechanics near the quantum limit*, Nature Communications **3**, 987 (2012).
- [76] M. C. Kuzyk and H. L. Wang, *Controlling multimode optomechanical interactions via interference*, Physical Review A **96**, 023860 (2017).
- [77] M. C. Kuzyk, S. J. van Enk, and H. L. Wang, Generating robust optical entanglement in weak-coupling optomechanical systems, Physical Review A 88, 062341 (2013).
- [78] Y. D. Wang and A. A. Clerk, *Using dark modes for high-delity optomechanical quantum state transfer*, New Journal of Physics **14**, 105010 (2012).
- [79] A. Uhlmann, *The transition probability in the state space of a*-algebr*, Reports on Mathematical Physics **9**, 273 (1976).
- [80] G. Balasubramanian, P. Neumann, D. Twitchen, M. Markham, R. Kolesov, N. Mizuochi, J. Isoya, J. Achard, J. Beck, J. Tissler, V. Jacques, P. R. Hemmer, F. Jelezko, and J. Wrachtrup, *Ultralong spin coherence time in isotopically engineered diamond*, Nature Materials **8**, 383 (2009).
- [81] D. A. Golter, T. K. Baldwin, and H. L. Wang, *Protecting a Solid-State Spin from Decoherence Using Dressed Spin States*, Physical Review Letters **113**, 237601 (2014).
- [82] X. K. Xu, Z. X. Wang, C. K. Duan, P. Huang, P. F. Wang, Y. Wang, N. Y. Xu, X. Kong, F. Z. Shi, X. Rong, and J. F. Du, *Coherence-Protected Quantum Gate by Continuous Dynamical Decoupling in Diamond*, Physical Review Letters **109**, 070502 (2012).
- [83] W. F. Koehl, B. B. Buckley, F. J. Heremans, G. Calusine, and D. D. Awschalom, *Room temperature coherent control of defect spin qubits in silicon carbide*, Nature **479**, 84 (2011).
- [84] A. G. Fowler, A. M. Stephens, and P. Groszkowski, *High-threshold universal quantum computation on the surface code*, Physical Review A **80**, 052312 (2009).